Nanotechnology **22** (2011) 355301 (8pp) doi:10.1088/0957-4484/22/35/355301

One-step substrate nanofabrication and patterning of nanoparticles by lithographically controlled etching

M Bianchi[1], D Limones Herrero[1], F Valle[1], P Greco[2], G M Ingo[3], S Kaciulis[3], F Biscarini[1] and M Cavallini[1]

[1] CNR, Institute of Nanostructured Materials, Via P Gobetti 101, 40129 Bologna, Italy
[2] SCRIBA Nanotecnologie S.r.l., Via P Gobetti 52/3, 40129 Bologna, Italy
[3] CNR, Institute of Nanostructured Materials, 00015 Monterotondo Stazione, Roma, Italy

E-mail: m.cavallini@bo.ismn.cnr.it

Received 3 June 2011, in final form 14 July 2011
Published 5 August 2011
Online at stacks.iop.org/Nano/22/355301

Abstract
We propose an integrated top-down and bottom-up approach to single-step nanofabrication of complex nanostructures made of different materials. The process, termed lithographically controlled etching (LCE), starts with a drop of an etching solution cast on the surface to be patterned. By placing a polymeric mold on the substrate, the stamp protrusions come into contact with the surface, thus protecting it, whereas the surface beneath the mold recesses is exposed to a thin layer of etching solution, allowing the surface to be etched. By dispersing nanoparticles into the etching solution, these can be deposited and self-organize in the recesses on the substrate as these are excavated. We demonstrate here the fabrication of complex structures and nanowires 30 nm wide. Moreover, by exploiting capillary forces, it is possible to deposit nanoparticles at precise positions with respect to optically addressable microstructures, thus realizing a multiscale functional pattern.

S Online supplementary data available from stacks.iop.org/Nano/22/355301/mmedia

(Some figures in this article are in colour only in the electronic version)

1. Introduction

In recent years a vast range of insulating, semiconducting and metallic nanoparticles have been synthesized in a variety of forms and shapes [1, 2]. These nanoparticles exhibit exceptional physical properties that can be used to realize novel devices. In order to exploit their functionalities, a persistent challenge has been their connection from devices to the outside world. Integration of nanoparticles into device structures [3, 4] requires the precise control of the size and positions of nano-objects on a patterned substrate [5–8]. Either the functional materials or the substrates can be independently nanostructured by several efficient methods such as soft lithography [9–11], transfer printing [12, 13], nano-imprinting [14], lithographically controlled wetting [15, 16] and scanning probe lithography [17], while inorganic substrates have been fabricated by photolithography [18, 19], electron beam lithography [20], nano-imprinting [21] and other methods [22, 23]. However, the application of these methods requires first the fabrication of the substrate followed by a second step with the additive deposition of nanomaterials. Although combinations of top-down and bottom-up processes have been proposed for several applications [24], no established methods have led to the simultaneous patterning of the substrate and the functional material. A single-step method able to pattern a substrate and deposit or self-assemble addressable functional material is thus highly desirable [25]. It should be recognized that many devices based on organic and hybrid materials are fabricated on inorganic (e.g. Si/SiO_2) substrates and test beds [26]. Here we propose a parallel fabrication process, termed lithographically controlled etching (LCE), which enables one-step fabrication of organic or hybrid functional nanostructures on inorganic substrate, integrating in the same process both top-down and bottom-up approaches [27]. LCE is suitable for large area nano-patterning and is sustainable because of its simplicity, speed and versatility. By exploiting the self-organization

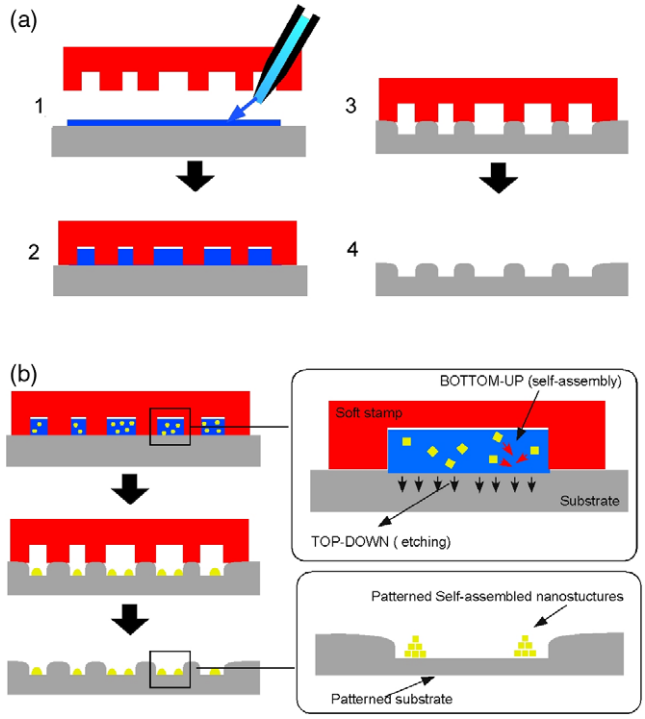

Figure 1. (a) Schematic illustration of the lithographically controlled etching (LCE) process. (b) LCE combined with solute deposition.

properties of functional materials in confined meso- and nanoscopic cavities created on the surface, the fabrication of nanometer-size structures in a few minutes and in a single step can be achieved.

2. Results and discussion

2.1. LCE technique

In LCE (figure 1(a)), a drop of etching solution (ES) is spread on a surface. When a polymeric mold is placed on the substrate, the stamp protrusions come into contact with the surface, thus protecting the surface underneath and giving rise to cells under the recesses of the stamp motif [28]. The ES reacts with the surface only under the recesses and when the process is terminated a patterned surface is obtained, being a negative replica of the stamp. The initial spreading of the solution on flat surfaces before placing the stamp gives rise to a homogeneous distribution, which produces a corresponding homogeneous modeling of the surface. This procedure can only be applied to mildly aggressive ESs, since for a few seconds the solution reacts with the surface without any spatial confinement. Therefore, only ESs with etching rates <25 nm min^{-1} are suitable for LCE. The cell volume, the concentration of the ES and the time of application determine the etched thickness and size. Since the process does not rely on specific interactions between the solution and the surface, LCE is of general application to a large variety of etchable substrates and soluble materials.

Here LCE has been applied to a thermal silicon oxide substrate (SiO_2/Si, nominal oxide thickness $\sim$200 nm) using HF as the etching solution.

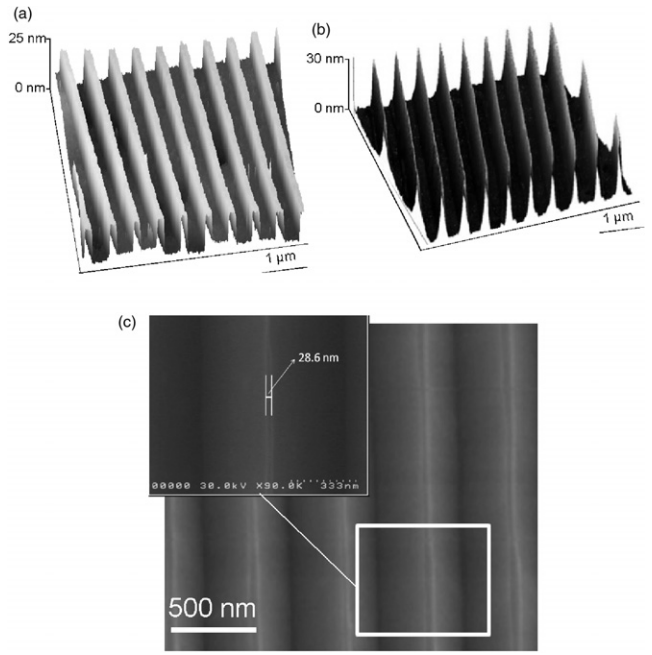

Figure 2. 3D AFM images of (a) SiO_2 nanowires (width 216 ± 11.5 nm) printed by LCE and (b) SiO_2 nanowires after bulk etching (width 91.3 ± 4.5 nm). (c) SEM image of Si nanowires (width 28 ± 2.5 nm) fabricated by applying 3% KOH bulk etching on SiO_2 nanowires as in (b). The inset shows a single nanowire in more detail.

The etch rate of thermal oxide using different HF dilutions at room temperature is nearly linear with HF concentration in a fairly large concentration range [29]. The etching reaction (equation (1)) produces, other than water, only a volatile species, thus it does not leave any residual compound on the surface:

$$SiO_2\ (s) + 4HF\ (aq) \rightarrow SiF_4\ (g) + 2H_2O\ (l). \qquad (1)$$

Figure 2(a) shows a 3D AFM image of parallel SiO_2 stripes obtained by LCE using a stamp made of parallel lines (320 nm FWHM and 540 nm pitch, HF 0.4%).

The control of the etching time allows a fine-tuning of the height and size of the linear structures. For example, by applying a further etching treatment in bulk (4 min, HF 4%) to SiO_2 sub-micrometric wires as in figure 2(a), arrays of SiO_2 nanowires can be fabricated, showing a mean width of <100 nm and a length of up to few millimeters (figure 2(b)). It is worth noting that by applying a further anisotropic etching using a KOH 3% solution to etch the underlying Si and eliminating the residual SiO_2 with concentrated HF (40%) the fabrication of Si nanowires of <30 nm width is easily achievable (figure 2(c)).

Figure 3(a) shows the AFM image of a square grating obtained by iterating the LCE process twice on Si/SiO_2 substrate, by rotating the stamp by 90° before the second etching treatment. Due to the nature of the process, the depths of the two groups of perpendicular stripes are slightly different. A further etching with KOH yields a grating pattern with homogeneous Si stripes (figure 3(b)).

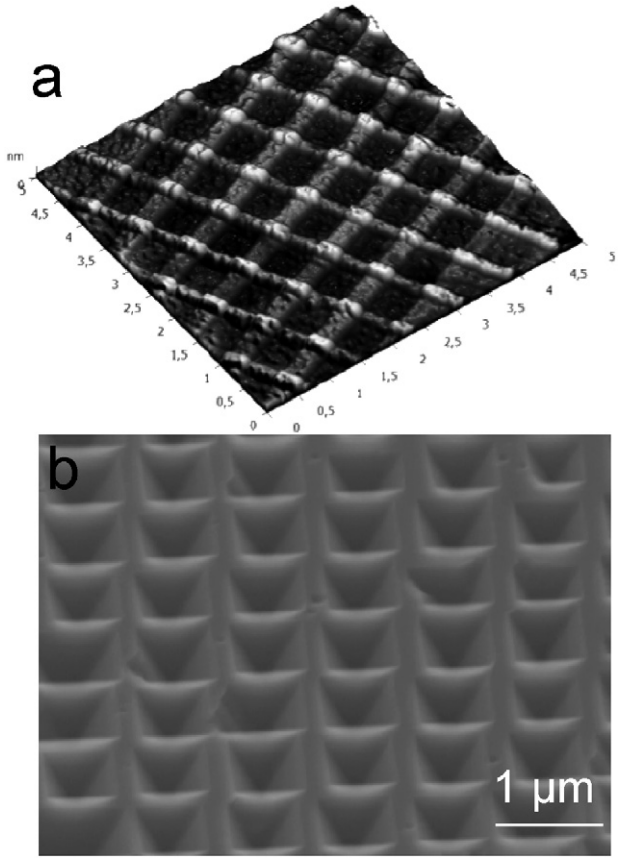

Figure 3. (a) 3D AFM image of a square grating obtained by iterating the LCE process on the SiO_2 surface by rotating the stamp by 90° after the first etching. (b) SEM image of crossed nanowires obtained from (a) by applying a further anisotropic etching using KOH.

Table 1. Pitch and FWHM values of stamps showing linear patterns.

	Stamp A	Stamp B	Stamp C
Pitch (nm)	1500	710	520
FWHM (nm)	600	420	320

Characteristic features (full width at half maximum (FWHM), pitch, stripe density, duty cycle, aspect ratio) of linear patterns fabricated by LCE using stamps with different pitches and FWHMs (table 1) are summarized in table 2. The duty cycle is defined as the percentage ratio between the FWHM and the pitch. The aspect ratio in this case is defined as the ratio between the FWHM and the height of the printed stripes.

Sample 1 was been obtained from stamp A, sample 2 from stamp B, sample 3 from stamp C and sample 4 (SiO_2 nanowires) from bulk etching after the first LCE treatment with stamp C.

Table 2 indicates that by the LCE technique it is possible to fabricate linear patterns with high stripe density (20 000 cm^{-2}), very low duty cycle (17.5%, with the printed stripe being about six times smaller than the pitch) and aspect ratio of ∼2.5. LCE was successfully applied for the fabrication of structures (grooves) with sizes ranging from <100 nm to 50 μm (see the supplementary information (SI) available at stacks.iop.org/Nano/22/355301/mmedia) and to fabricate nanostructures in relief of <30 nm width. Above 50 μm the structures fabricated by LCE become less homogeneous and the sagging of polydimethylsiloxane (PDMS), although less relevant than in traditional soft lithography due to the presence of the uncompressible solution inside the channels (see figure 1 and section 4.4), starts to be a major problem.

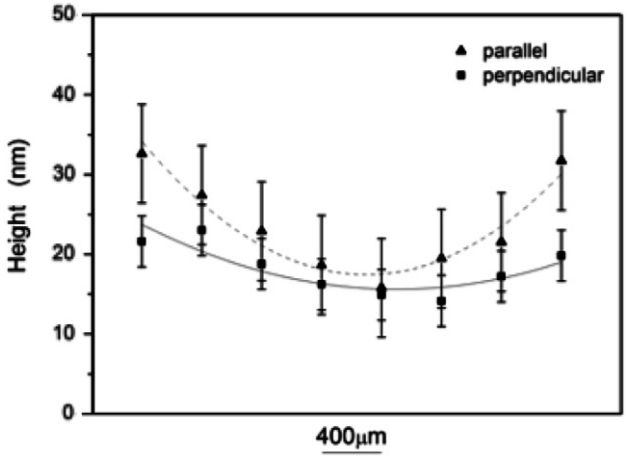

Figure 4. Representative height profile of a printed feature at the macroscale measured along the directions perpendicular (▲) and parallel (■) to the wires. The mean value of the height dispersion is 3.2 nm.

Table 2. Characteristic sizes of printed features. Note that in sample 4 etching was applied two times.

Sample	FWHM (nm)	Pitch (nm)	Duty cycle (%)	Aspect ratio
Sample 1	630	1496	42.1	12.4:1
Sample 2	296	709	29.2	9.6:1
Sample 3	216	520	41.5	7.7:1
Sample 4	91	520	17.5	2.5:1

2.2. Statistical analysis of the samples' homogeneity

The homogeneity of the samples over large areas (3 × 3 mm^2) has been assessed by statistical analysis of the characteristic features of samples made of parallel wires (750 nm pitch and 550 nm width) that we consider representative for LCE. The size and height of the printed features have been extracted from AFM topographic images (IAProject, 'Histogram' function, NT-MDT, Moscow, Russia) acquired every 400 μm in the parallel and perpendicular directions with respect to the wires' orientation. The movement along each direction was achieved by rotating micrometric screws beside the AFM head. Figure 4 shows a representative profile of the height of etched features measured as above.

The protrusion height results as systematically slightly higher (∼10%) at the borders, but there is a large and predominant homogeneous area (>96%) where the mean height does not change significantly (significance level in t-test, $p > 0.05$, GraphPad Software).

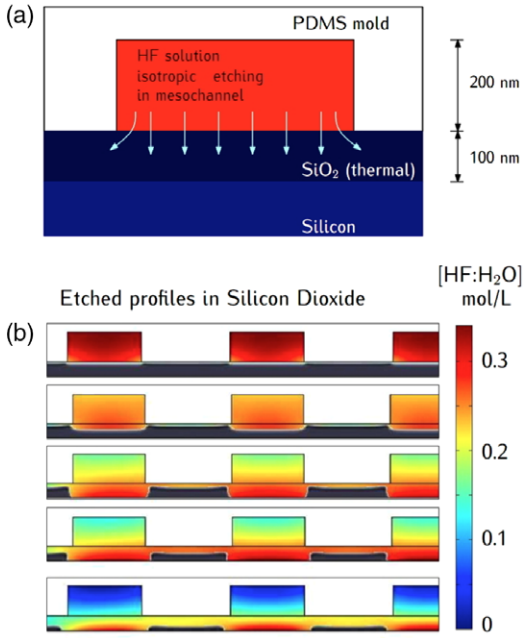

Figure 5. LCE simulation by finite element modeling. (a) Scheme of the subdomains used in the finite element calculation. The HF solution reacts with the underlying silicon dioxide surface isotropically, although confined by the PDMS mold. (b) Time evolution of the concentration of the etching solution within the mesochannel section. At the beginning, a thin film of SiO_2 is etched in correspondence with the channel cavities; after the etching, the concentration is higher toward the surface. The simulation has been carried out with a 25 nm min^{-1} etching rate.

2.3. Simulation by finite element modeling

Simulation of the isotropic HF etching process in a confined environment has been carried out by finite element modeling to get new insight into the process. The solution provides the flow dynamics within the channels employing the experimental etching rates reported in the SI (available at stacks.iop.org/Nano/22/355301/mmedia).

The simulation starts ($t = 0$) as the stamp is placed in contact with the surface, assuming a rectangular (600×200 nm^2) channel section (figure 5(a)). The surface tension term has been included in the Navier–Stokes equation to calculate the evolution of the profile of the SiO_2 surface. The reaction, taking place on the surface, generates gaseous SiF_4 [30] which reduces the overall HF density near the etched region by approximately 10%. A buoyancy effect allows the calculation of the fluid streamline field [31].

The concentration of HF within the channels has been estimated by a convection and diffusion regime, using the velocity field obtained from the Navier–Stokes equation. During the process, while the volume of the cell is increasing, the HF concentration decreases because the chemical reaction consumes HF (see equation (1)), creating a gradient of concentration, which reduces the etching rate (figure 5(b)). From the results, it appears that at later stages there is a polarization of the HF concentration toward the surface due to the structure of the substrate. While at the beginning of the process the surface is preferentially etched in correspondence with the channel cavities and the etching solution concentration is homogeneous, after a few seconds also the regions under the stamp protrusion are partially etched (figure 5(b)). This process limits the possibility for LCE to be applied for the fabrication of sub-100 nm half-pitch patterns with a reasonable (>2) aspect ratio.

The simulation shows that the isotropic etching of HF is hindered by the sub-micrometric size of the channels, allowing an improvement of the resolution of the printed features with respect to conventional etching.

2.4. LCE integrated with nanoparticle deposition

Although the examples reported up to this point only deal with a patterned surface, an attractive feature of LCE is the deposition of functional materials and/or nanoparticles (NPs) at the same time as the etching process, simply by starting from a solution or dispersion of the ES and the functional materials. The only limitation is that the solute must be resistant to the ES. Effectively LCE deposition reproduces conditions similar to unconventional wet lithography [15, 32]; in particular it resembles the condition occurring in the last step of micromolding in capillaries [33]. As the critical concentration in the solution is reached, the solute precipitates from the solution onto the substrate, giving rise to a structured thin film replicating the stamp recesses. Using a sufficiently concentrated solution, i.e. the solution reaches supersaturation when the volume of the solution is comparable with the volume of the cell, a homogeneous thin film of the dispersed material can be obtained. On the other hand, when using a diluted solution, the supersaturation is reached at a later phase of the evaporation, i.e. when the volume of the solution becomes smaller than the volume of the cell. In this regime the capillary forces pin the solution to form menisci around the stamp protrusions. The amount of deposited NPs is controlled by adjusting their concentration in the initial solution. An intriguing outcome of LCE combined with NP deposition appears in figure 6 where stamps with a low density (~ 1 μm^{-2}) of oval-shaped sub-micrometric features of different lengths are used, i.e. the logic structures obtained by employing a stamp of a replica of a commercially written digital video disk (DVD)). Using a very diluted solution of gold nanoparticles (0.4 NPs μm^{-2}, mean $\varnothing \sim 15$ nm), the probability of finding a gold NP close to a micrometric structure is proportional to the length of the structures. Since the meniscus at the later stage of the evaporation drives the solution around the protrusions in contact with the substrate [15], the use of a stamp containing a number of micrometric structures comparable with the number of NPs permits the positioning of a limited number of NPs only around the longer structures. Furthermore, due to the meniscus effect during the last step of solvent evaporation [15] the NPs are placed at the middle of the microstructure's length.

In this manner it is possible to deposit NPs mostly at the middle edge of the larger microstructures. Since the latter can be identified by an optical microscope, the nano-objects become 'optically addressable' (a $50\times$ objective is sufficient to resolve them) for further characterization or exploitation of their functionality. We have estimated from the analysis

Table 3. Atomic concentrations (%) and BE values (eV) of the chemical species on the surface of different representative samples.

	Peak									
	C1	C2	C3	F 1s	O 1s	Si1	Si2	Si3	N 1s	Au 4f7
Sample										
1	3.8	1.4	0.6	0.6	60.8	29.5	3.3	0	—	—
1a	20.5	7.2	0	0.4	51.6	20.0	0	0	0.2	0.085
2	24.6	2.9	0.8	0.4	40.1	14.7	2.6	13.9	—	—
3	7.7	0.5	0	0.8	56.8	34.1	0	0	—	0.1
4	19.9	1.5	1.0	—	47.2	24.7	0	5.3	0.1	0.2
1	3.8	1.4	0.6	0.6	60.8	29.5	3.3	0	—	—
BE	285.0	≈287	≈289	688	≈533	≈103.4	≈105.4	≈102	≈400	84.0

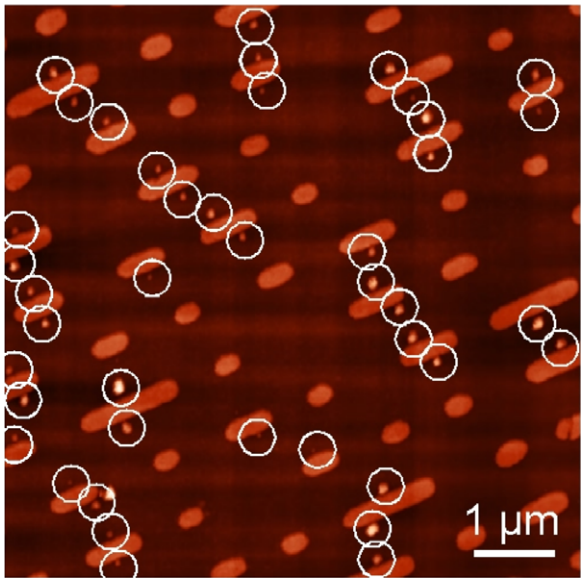

Figure 6. LCE combined with gold NP deposition. AFM images of low density (∼1 NPs μm^{-2}) NPs deposited next to logic structures, scale bar 10 μm, z-range 0–50 nm. The number of NPs is comparable with the number of stamp protrusions. The white circles indicate the NPs that are preferentially self-positioned in the middle of the longer (>500 nm) structures fabricated by LCE.

of about 100 structures that under optimized conditions more than 98% of NPs are placed at the middle positions of printed structures longer than 500 nm with an accuracy of about ±170 nm.

The chemical composition of the surface, as well as the lack of damage of the NPs, and thus the preservation of their functionality after processing, have been assessed by x-ray photoelectron spectroscopy and UV–vis absorption spectroscopy.

2.5. X-ray photoelectron spectroscopy

The atomic concentrations of constituent elements and the binding energy (BE) values of the main XPS peaks, including their synthetic components obtained by peak fitting, have been collected with an ESCALAB MkII (VG Scientific, UK) spectrometer and are presented in table 3.

Sample 1 and sample 1a are the reference samples: untreated SiO_2/Si wafer and the SiO_2/Si wafer with Au NPs (drop casting) respectively; sample 2 is the LCE treated SiO_2/Si wafer; samples 3 and 4 are the LCE and lithographically controlled wetting (LCW) treated SiO_2/Si wafers with Au NPs, respectively. Sample 4 has been introduced to assess the effect of HF on the chemical composition of the surface in the presence of Au NPS (sample 3), by comparing the latter with a sample prepared following a normal LCW deposition (thus using water rather than HF).

As can be inferred from table 3, the surface of the untreated reference sample (sample 1) is characterized by a quasi-stoichiometric SiO_2 (Si1 and O peaks, 1:2) with a very low amount of contaminants (C and F). Only a small part of silicon (Si2) results in being bonded in some silicate and/or in some compound containing Si–C–F. Hence the initial cleaning protocol of the silicon wafer (see section 4) has to be considered efficient. A similar composition has been detected for sample 1a, where the presence of deposited Au NPs is revealed along with contaminants (C and N) originating from the nanoparticle organic ligand (mainly sodium citrate), thus modifying the stoichiometry of the silicon oxide surface.

LCE treated wafers (samples 2 and 3) exhibit similar compositions with a mild presence of Si suboxides in the sample without Au NPs (sample 2). The smaller percentage of C contaminants in sample 3 with respect to sample 1a can be ascribed to a partial elimination of the Au NPs' organic ligand by HF. This hypothesis is confirmed also by the data of sample 4, in which, in the absence of HF, the presence of C contaminant is significant.

Moreover, the low signal of N 1s at BE ≈ 400 eV, registered in samples 1a and 4, that indicates the presence of adsorbed amine groups [34] probably coming from the organic ligand, is not present in sample 3. In figure 7, the characteristic XPS peaks of sample 3 are reported.

The main component C1 of C 1s (see figure 7(b)) is attributed to the most common C–C and C–H bonds, whereas the low signals of C2 and C3 can be assigned to hydroxylic CH–OH and carboxylic O=C–OH bonds, respectively [35], attributed to the NP solution. The spectrum of Au 4f, composed of a typical spin–orbit split doublet, is shown in figure 7(c) (sample 4). These peaks correspond to metallic gold Au^0 at BE = 84.0 and 87.7 eV. The positive Au species, which can be found in the case of NPs covered with a positively charged shell [36, 37], were completely absent in our samples. The low signal of N 1s at BE ≈ 400 eV, registered in samples 1a and 4, indicates the presence of adsorbed amine groups [34].

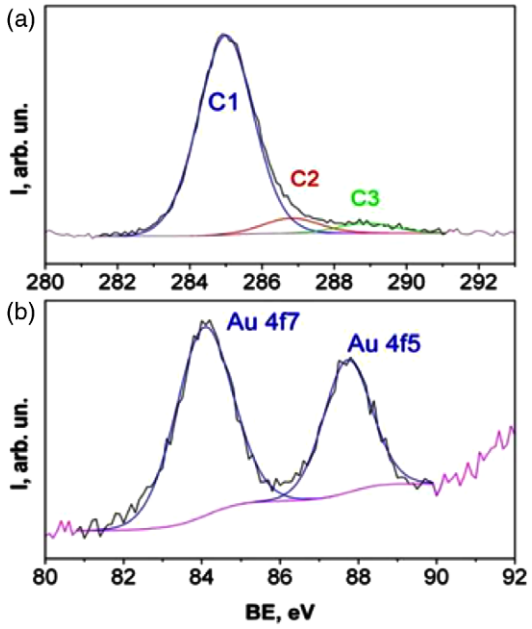

Figure 7. XPS spectra of (a) the C 1s and (b) the Au 4f regions of sample 3 prepared by LCE with Au NPs.

No sub-products derived from the etching treatment were produced on the SiO_2 substrates.

2.6. UV–vis absorption spectroscopy

Absorption spectra of processed NPs drop cast both from water solution and from 0.4% HF solution have been recorded by a Lambda 950 spectrophotometer (PerkinElmer, USA).

For this characterization 0.6 ml of Au NP solution was cast on quartz circular cylinders (diameter $\sim$ 1 cm, thickness $\sim$ 3 mm) through consecutive depositions, and dried at room temperature after each deposition. Both absorption spectra exhibited the typical absorption peak of Au NPs at around 530 nm, which is characteristic of isolated gold nanoparticles of 10–15 nm diameter (figure 8) [38].

In both cases, the two spectra show a considerable spreading in the range 530–800 nm, which indicates the presence of chains or aggregates of gold nanoparticles (expected when using these concentrations).

It can be concluded that no relevant effect due to the process has been produced, since a partial aggregation of NPs was already present in the starting material.

Finally, the measurements of absorption spectroscopy prove that LCE does not alter the macroscopic functionality of Au NPs.

3. Conclusions

In conclusion, a new robust soft lithography fabrication technique named lithographically controlled etching integrating both top-down (confined etching) and bottom-up (nanoparticle self-assembly) approaches, has been developed. The ability of LCE to fabricate micro- and nanostructures, down to sub-30 nm nanowire arrays, over macroscopic areas in a fast and reliable way has been demonstrated. We proved that functional NPs can be deposited by LCE at addressable positions by a single-step process designed for transferring micrometric markers. The possibility of depositing functional NPs within the cavities of the pattern in a controlled manner and in a single step, thus surpassing the state of the art fabrication techniques, makes it suitable for biomedical sensing [39], optoelectronics and data storage applications [40].

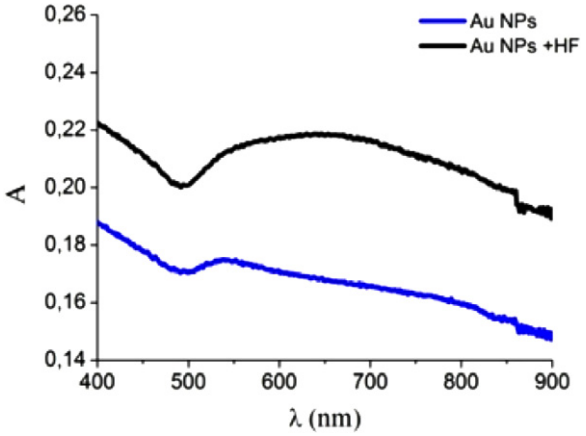

Figure 8. Absorption spectra of Au NPs drop cast from water solution (blue curve) and processed in 0.4% HF (black curve).

Here LCE has been applied mainly to Si/SiO_2 substrates and Au NPs as functional materials, but we have successfully extended the process to a wide range of technologically relevant substrates such as glass, TiO_2, manganites [41] and $SrTiO_3$, and other functional materials [42] such as magnetic materials [32, 43], organic semiconductors [44] and supramolecules [45].

4. Experimental section

4.1. Substrates

The substrates (Fondazione Bruno Kessler, Trento, Italy) consisted of an 8×8 mm^2 piece of silicon (Si⟨100⟩ n-doped with Sb, resistivity 0.01–0.03 Ω cm) covered by 200 nm of thermal SiO_2. Samples were cleaned by rinsing for 2 min in acetone (Aldrich chromatography quality) and 2 min in 2-propanol (Aldrich spectroscopic grade quality) and dried with N_2.

An air plasma treatment (Pelco easiGlow, USA) was performed ($t = 15$ min, $i = 30$ mA) to further clean the surface by eliminating all the residual organic compounds. The cleaned substrate resulted in a flat surface (RMS roughness $= 0.25 \pm 0.01$ nm) showing a water contact angle of $\theta_c = (61.8 \pm 1.5)°$.

4.2. Stamps

The elastomeric polydimethylsiloxane (PDMS, Sylgard 184, Dow Corning) stamps were prepared by replica molding of commercial masters made of silicon (SCRIBA Nanotecnologie, Bologna, Italy) by mixing the curing agent with the PDMS at 1:10 (v/v) and degassing for 30 min to eliminate

air bubbles. The curing process was carried out for 3 h at 90 °C. Once cured, the replica was gently peeled off from the master. The stamp motifs consisted of parallel lines with different periodicities (see the SI available at stacks.iop.org/Nano/22/355301/mmedia), logic structures (prepared by replica molding of blank or written Digital Versatile Disk support), arrays of holes and a CNR logo (for details, see the SI available at stacks.iop.org/Nano/22/355301/mmedia).

4.3. Au nanoparticles

Commercial SPI-Mark™ unconjugated gold colloidal suspension (1 g l^{-1}, mean diameter < 15 nm, SPI supplies Inc., USA) was used to demonstrate the capability of the LCE technique to deposit material during the etching process.

Solutions. Solutions were prepared starting from HF (Sigma Aldrich 40% v/v) or KOH (Sigma Aldrich 99% purity) diluted in electronic-grade water (milli-pure quality). For the etching experiments without Au NPs, the final HF concentration was 0.4%. For the NP deposition experiments, the NPs were diluted 1:10 in water and mixed with HF 4% (HF:NPs 1:10 v/v), thus the final HF concentration was kept equal to that used in the experiments without NPs. For SiO_2 nanowire fabrication the samples obtained by LCE were treated in bulk 4% HF solution for 4 min.

For Si nanowire fabrication the samples obtained by LCE were treated in bulk 3% KOH (w/w) solution for 40 min.

4.4. LCE general procedure

In LCE, a drop of etching solution (ES) is spread on a surface. A polymeric mold with geometrical features in the bottom part is then placed on the substrate. The stamp protrusions come into contact with the surface and protect the surface underneath, while the ES etches the unprotected areas. In order to prevent the stamp from floating over the mold, resulting in the inhomogeneous height of the printed features, a low pressure of imprinting can be applied ($\sim$50 g cm^{-2}) by tuning the stamp mass.

4.5. Atomic force microscopy

AFM images were recorded by a commercial AFM (NT-MDT Smena) operated in air, in semi-contact mode (relative humidity 55%). Single crystal silicon, n-type, 0.01–0.025 Ω cm, antimony-doped NSG10 cantilevers with a typical tip curvature radius of 10 nm were used. All the images were unfiltered, only a line-by-line background subtraction was performed to remove trend effects by NT-MDT image treatment software.

4.6. X-ray photoelectron spectroscopy

XPS was performed in order to assess the absence of etching residues on the surface and the presence of metal nanoparticles. These measurements were carried out by using an ESCALAB MkII (VG Scientific, UK) spectrometer equipped with a standard Al Kα excitation source and a five-channel detection system. Photoelectron spectra were collected at 20 eV constant pass energy of the analyzer and a base pressure in the analysis chamber of 10^{-8} Pa. The spectra were processed by Casa XPS v. 2.2.84 software, using a peak-fitting routine with symmetrical Gaussian–Lorentzian functions. The background was subtracted from the photoelectron spectra using the Shirley method.

Acknowledgments

We thank Valeria Fattori for the adsorption spectroscopy measurements. This work was part of the ESF–European Young Investigators Awards Scheme, DYMOT. Partial support by EC FP7 ONE-P Large Scale project no. 212311 is also acknowledged.

References

[1] Murray C B, Kagan C R and Bawendi M G 2000 *Annu. Rev. Mater. Res.* **30** 545–610
[2] Manna L, Scher E C and Alivisatos A P 2002 *J. Cluster Sci.* **13** 521–32
[3] Nie Z H, Petukhova A and Kumacheva E 2010 *Nature Nanotechnol.* **5** 15–25
[4] Huang Y, Duan X F, Wei Q Q and Lieber C M 2001 *Science* **291** 630–3
[5] Wiley B J, Qin D and Xia Y 2010 *ACS Nano* **4** 3554–9
[6] Vossmeyer T, Jia S, DeIonno E, Diehl M R, Kim S H, Peng X, Alivisatos A P and Heath J R 1998 *J. Appl. Phys.* **84** 3664–70
[7] Cheng W, Park N, Walter M T, Hartman M R and Luo D 2008 *Nature Nanotechnol.* **3** 682–90
[8] Kim H, Kim J, Yang H, Suh J, Kim T, Han B, Kim S, Kim D S, Pikhitsa P V and Choi M 2006 *Nature Nanotechnol.* **1** 117–21
[9] Xia Y N and Whitesides G M 1998 *Angew. Chem. Int. Edn* **37** 551–75
[10] Cavallini M, Murgia M and Biscarini F 2001 *Nano Lett.* **1** 193–5
[11] Greco P *et al* 2008 *J. Am. Chem. Soc.* **130** 1177–82
[12] Serban D A, Greco P, Melinte S, Vlad A, Dutu C A, Zacchini S, Iapalucci M C, Biscarini F and Cavallini M 2009 *Small* **5** 1117–22
[13] Meitl M A, Zhu Z T, Kumar V, Lee K J, Feng X, Huang Y Y, Adesida I, Nuzzo R G and Rogers J A 2006 *Nature Mater.* **5** 33–8
[14] Cedeno C C *et al* 2002 *Microelectron. Eng.* **61–62** 25–31
[15] Cavallini M, Albonetti C and Biscarini F 2009 *Adv. Mater.* **21** 1043–53
[16] Cavallini M and Biscarini F 2003 *Nano Lett.* **3** 1269–71
[17] Salaita K, Wang Y and Mirkin C A 2007 *Nature Nanotechnol.* **2** 145–55
[18] Jaeger R C 2002 *Lithography. Introduction to Microelectronic Fabrication* (Englewood Cliffs, NJ: Prentice-Hall)
[19] Rogers J A, Paul K E, Jackman R J and Whitesides G M 1997 *Appl Phys. Lett.* **70** 2658–60
[20] Vieu C, Carcenac F, Pepin A, Chen Y, Mejias M, Lebib A, Manin-Ferlazzo L, Couraud L and Launois H 2000 *Appl. Surf. Sci.* **164** 111–7
[21] Chou S Y, Krauss P R, Zhang W, Guo L J and Zhuang L 1997 *J. Vac. Sci. Technol.* B **15** 2897–904
[22] Ahn H, Lee K J, Shim A, Rogers J A and Nuzzo R G 2005 *Nano Lett.* **5** 2533–7
[23] Cavallini M *et al* 2010 *Nanoscale* **2** 2069–72
[24] Henzie J, Barton J E, Stender C L and Odom T W 2006 *Acc. Chem. Res.* **39** 249–57
[25] Shim W, Braunschweig A B, Liao X, Chai J, Lim J K, Zheng G and Mirkin C A 2011 *Nature* **469** 516–20

[26] Klauk H 2010 *Chem. Soc. Rev.* **39** 2643–66
[27] Cavallini M, Facchini M, Massi M and Biscarini F 2004 *Synth. Met.* **146** 283–6
[28] Melucci M, Zambianchi M, Favaretto L, Palermo V, Treossi E, Montalti M, Bonacchi S and Cavallini M 2011 *Chem. Commun.* **47** 1689–91
[29] Williams K R, Gupta K and Wasilik M 2003 *IEEE J. Microelectromech. Syst.* **12** 761–78
[30] Knotter D M 2000 *J. Am. Chem. Soc.* **122** 4345–51
[31] Greco P *et al* 2008 *J. Am. Chem. Soc.* **130** 1177–82
[32] Cavallini M, Facchini M, Albonetti C and Biscarini F 2008 *Phys. Chem. Chem. Phys.* **10** 784–93
[33] Kim E, Xia Y N and Whitesides G M 1996 *J. Am. Chem. Soc.* **118** 5722–31
[34] Sylvestre J P, Poulin S, Kabashin A V, Sacher E, Meunier M and Luong J H T 2004 *J. Phys. Chem.* B **108** 16864–9
[35] Svorcik V, Hubacek T, Slepicka P, Siegel J, Kolska Z, Blahova O, Mackova A and Hnatowicz V 2009 *Carbon* **47** 1770–8
[36] Mazzaglia A, Scolaro L M, Mezzi A, Kaciulis S, De Caro T, Ingo G M and Padeletti G 2009 *J. Phys. Chem.* C **113** 12772–7
[37] Gillet J N and Meunier M 2005 *J. Phys. Chem.* B **109** 8733–7
[38] Duchesne L, Gentili D, Comes-Franchini M and Fernig D G 2008 *Langmuir* **24** 13572–80
[39] Valle F, Chelli B, Bianchi M, Greco P, Bystrenova E, Tonazzini I and Biscarini F 2010 *Adv. Eng. Mater.* **12** B185–91
[40] Cavallini M, Gomez-Segura J, Albonetti C, Ruiz-Molina D, Veciana J and Biscarini F 2006 *J. Phys. Chem.* B **110** 11607–10
[41] Leyva A G *et al* 2004 *J. Solid State Chem.* **177** 3949–53
[42] Cavallini M, Aloisi G, Bracali M and Guidelli R 1998 *J. Electroanal. Chem.* **444** 75–81
[43] Coronado E, Marti-Gastaldo C, Galan-Mascaros J R and Cavallini M 2010 *J. Am. Chem. Soc.* **132** 5456–68
[44] Surin M *et al* 2007 *J. Mater. Chem.* **17** 728–35
[45] Cavallini M, Lazzaroni R, Zamboni R, Biscarini F, Timpel D, Zerbetto F, Clarkson G J and Leigh D A 2001 *J. Phys. Chem.* B **105** 10826–30